

# Refined FEM Analysis of Steel-Concrete Composite Beam Subjected to Negative Bending and Axial Compressive Forces

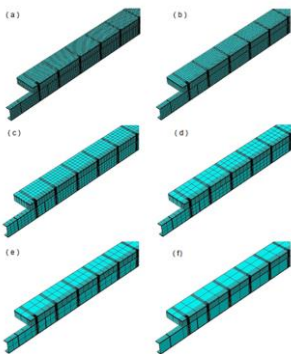
Mahesan Bavan<sup>a</sup>, Shahrizan Baharom<sup>a\*</sup>, Azrul A. Mutalib<sup>a</sup>

<sup>a</sup>Department of Civil and Structural Engineering, Universiti Kebangsaan Malaysia, Bandar Baru Bangi, Selangor, Malaysia

\*Corresponding author: shah@vlsi.eng.ukm.my

## Article history

Received :20 August 2013  
Received in revised form :  
25 September 2013  
Accepted :15 October 2013



## Abstract

This paper presents modelling techniques with finite element method (FEM) for a composite beam subjected to combined negative bending and axial compressive forces. Flexural behaviours of composite beam were thoroughly analysed to determine the ultimate limit state due to vertical and axial compressive forces. Failure state of composite beam was revealed by the level of axial compressive forces and reduced negative moment due to axial compressive forces. The results obtained from FEM analysis were compared with the results of experimental analysis. Reliability agreement has been observed between the results of FEM and experimental analysis on ultimate state behavior and failure modes. Detailed numerical techniques such as loading strategies in combined vertical and axial compressive directions and potential convergence problems due to complicated contacts between the material components are discussed in this paper. Finally simplified numerical techniques for uncertainties in axially compressed composite beam subjected to negative bending are suggested.

**Keywords:** Composite beam; numerical techniques; ultimate limit state behaviour; modes of failure; combined negative bending and axial compressive force

© 2013 Penerbit UTM Press. All rights reserved.

## 1.0 INTRODUCTION

To date, most studies have been focused in the effects of combined axial forces on composite beam [1-14]. The performance of composite beams under combined bending and torsion was examined by Nie *et al.* [1]. They proposed mathematical models to predict the resistance of composite steel concrete composite beams under flexure and torsion. The effects of torsion on straight and curved beams were reported with experimental analysis by Tan *et al.* [2, 3]. They also presented the design models for the straight and curved composite beam subjected to combined flexure and torsion. Mirza *et al.* [4] studied the effects of the combination of axial and shear loading on the headed stud steel anchors. They brought that the strength and ductility of composite beams are influenced by non-linearity of shear connections and further, they concluded that the axial tensile capacity is reduced with an increase in slab thickness. Elghazouli *et al.* [5] studied the inelastic behaviour of composite members under combined bending and axial loading. They found by their analytical studies that the bending moment capacity is influenced by axial load levels with local buckling effects. Loh *et al.* [6-7] conducted tests and analytically studied the effects of partial shear connection in the hogging moment regions of composite beams. They concluded that the beams

contain partial or full shear connection, are almost having similar behaviours and there is slight reduction in ultimate strength in terms of benefits in ductility.

The effects of axial tension on the hogging-moment regions of composite beam were investigated by Vasdravellis *et al.* [8]. Their studies brought with design models that low level of axial tensile forces are not given the effects in the negative moment capacity. Further, the negative moment capacity is reduced with increasing the level of tension in high level of axial tensile forces as well. Vasdravellis *et al.* [9] studied the effects of axial tension on the sagging-moment regions of composite beams. Their research provided experimental data and they concluded with design models that the presence of axial tensile forces acting in the steel beam section reduces the moment capacity of composite beam. Baskar and Shanmugam [10] presented results from a series of tests on steel-concrete composite plate girders subjected to combined shear and bending. They found that the composite action is more effective in the girders subjected to combined shear and positive bending comparing with pure shear loading. Meantime, they revealed further that the composite action is less effective in girders subjected to combined shear and negative bending.

Many challenges have been encountered during modelling and analysis of steel-concrete composite beams where the

beams are applicable with combined negative bending and compressive forces. Design engineers face practical issues by short of design models for more general cases of this specific issue. The examples of such applicable cases are beams, which are located on windward side of high-rise frames either subjected to inclined members or affected by diaphragm effects. The phenomenon in interaction and shear transmission between structural steel and reinforced concrete components is unknown constraints due to excess axial compressive forces. Investigation of this phenomenon, which will carry the composite beam to non-linear response and fracture mechanisms of the body of material components, must properly represent to solve those challenges. Specific concerns are necessary to be overcome in the failure modes with different local effects and ultimate limit states owing to compressive axial loads on steel concrete composite beams. In this perspective circumstances, the analysis is necessary to be stressed.

Currently, design models are not existed in design guidelines especially in Eurocode and British Standards for composite beams subjected to combined axial compressive forces and bending moments [11]. A design model to predict ultimate limit state of such composite beams was proposed very recently by Vasdravellis *et al.* [12]. Moreover, Vasdravellis *et al.* [13] reported that there is reduction in moment capacity due to additional axial compressive forces on steel section of composite beam subjected to negative bending. However, it should be noted that the concept of composite beam with combined binary axial forces to be implemented in order to obtain reliable results for various general cases.

There are limited research studies in the finite element modelling with different bimodular behaviour of material responses due to combined axial forces. Nonlinear analysis of composite beams subjected to combined flexure and torsion was studied with three dimensional finite element analysis by Tan *et al.* [14]. Tahmasebinia *et al.* [15] reported in probabilistic three-dimensional finite element study on composite beam with steel trapezoidal decking. Three dimensional FEM models of studs connected with steel-concrete composite girders subjected to monotonic loading were reported by Qureshi *et al.* [16]. Thevendran *et al.* [17] developed FEM models to predict the behaviour of curved in plane composite steel-concrete composite beams. The enhancement in computer and software technology has been improved nowadays and thus, longer computational time and more complex post-processing results are possible to get in an easiest way of accurate predictions.

This paper deals with detailed post-processing of the results and global non-linear structural behaviour of steel-concrete composite beam subjected to combined negative bending and axial compressive forces by using FEM. Even though, FEM model of composite beam has been published by Vasdravellis *et al.* [12-13], the shear stud was modeled with spring elements by force-slip law. The surface contact properties and uplift behaviour of material components such as steel beam and concrete slab were eliminated in their previous studies. Thus, those were included by using solid shear studs in this paper where the control techniques was applicable with concerning on severe cracking of concrete in the region of surrounding the studs. Moreover, fractural behaviour of each material components were thoroughly investigated with simultaneous increments until the structure completely failed. The control methods with concerning all material components specifically concrete, which is brittle material and leads to fail in a sudden drop of load carrying capacity, were particularly considered. Thus, a slow uniform displacement was necessary for the application of combined loadings of structure. Finally, the optimum rates of both combined vertical and axial

compressive loadings are suggested in this paper. Prediction of quasi-static solution, limited kinetic energy and force stabilities of applied and support reaction are also reported in this paper. In addition, this FEM provides ideas to extent more general cases for design parameters due to lack of researches and established design models in axial compressive loads on negative bending region of composite beams. Lastly, the best method of prediction through FEM is suggested to provide robust and stable solution procedure for composite beam subjected to negative bending and axial compressive forces.

## 2.0 EXPERIMENTAL REVIEWS

Four full scale specimens of composite beams were carried out for studies about combined negative bending and axial compressive loads on composite beam by Vasdravellis *et al.* [12-13]. The composite beam test arrangement is shown in Figure 1(a), which was a full scale composite beam 4500mm-length, 600mm-width and with a 203UB×133×30 universal beam section. Detailed cross section of composite beam is shown in Figure 2(a). The slab, depth was 120mm, which reinforced by 12mm bars in the longitudinal and transverse directions with spacing of 200mm and 120mm, respectively. Shear studs with 19mm in diameter and 100mm in height were welded with 400mm spacing and in a single line along the center of steel beam flange. Clear span between two roller supports was maintained at 4950mm in this specimen. The numbers of shear studs were designed by means of full shear interaction between slab and steel beam. Additionally, a group of three shear studs was welded at both ends of steel beam to avoid excessive slip as shown in Figure 2(b). Details of location of shear studs and applied load are indicated in Figure 3.

Both axial and vertical load were applied simultaneously by using load actuators specifically from four hydraulic actuators each 800kN and 200mm stroke to apply axial compression at east of beam and as well 1000kN and 250 mm stroke actuator to apply vertical force. Vertical load and axial load applications method are shown in Figure 1(b) and Figure 1(c), respectively. Two specimens CB1 and CB6 were particularly loaded vertically and pure axially, while the rest of four specimens CB2 to CB5 were tested with different combination of level of axial compression and vertical load until the failure occur in the material components. The failure state and mode of failure were recorded in each specimen and the values of axial load and moment combination were presented as ultimate limit state of the composite beam subjected to combined negative bending and axial compressive loads. The different levels of axial compression were purposely applied to predict the varied negative moment at each level of axial compression to the specimen CB2 to CB5. The summarizes of results of tested beams are shown in Table. 1.

The resulting bending moment was calculated by the following Equation (1).

$$M = \frac{P_v L}{4} + P_H e - M_{sw} \quad (1)$$

where  $P_v$  is the applied vertical force to the steel beam;  $P_H$  is the axial compressive force applied to the cross section of the steel beam;  $L$  is the clear span length between vertical supports;  $M_{sw}$  is the moment due to the self weight of the beam; and  $e$  is the eccentricity calculated by distance between plastic neutral axis of the composite beam and the pin of axial compressive load applicator.

Eccentricity  $e$  was determined by the following Equation (2).

$$e = \left( D_c + t_f + \frac{d_w}{2} \right) - y_c + \delta \tag{2}$$

where  $D_c$  is the slab thickness;  $t_f$  is the flange thickness;  $d_w$  is the height of the web;  $y_c$  is the depth of plastic neutral axis determined from the top of the slab; and  $\delta$  is the measured vertical deflection at the mid span.

Both axial and vertical load were applied simultaneously by using load actuators specifically from four hydraulic actuators each 800kN and 200mm stroke to apply axial compression at east of beam and as well 1000kN and 250 mm stroke actuator to apply vertical force. Vertical load and axial load applications method are shown in Figure 1(b) and Figure 1(c), respectively. Two specimens CB1 and CB6 were particularly loaded vertically and pure axially, while the rest of four specimens CB2 to CB5 were tested with different combination of level of axial compression and vertical load until the failure occur in the material components. The failure state and mode of failure were recorded in each specimen and the values of axial load and moment combination were presented as ultimate limit state of the composite beam subjected to combined negative bending and axial compressive loads. The different levels of axial compression were purposely applied to predict the varied negative moment at each level of axial

compression to the specimen CB2 to CB5. The summarizes of results of tested beams are shown in Table. 1.

The resulting bending moment was calculated by the following Equation (1).

$$M = \frac{P_v L}{4} + P_H e - M_{sw} \tag{1}$$

where  $P_v$  is the applied vertical force to the steel beam;  $P_H$  is the axial compressive force applied to the cross section of the steel beam;  $L$  is the clear span length between vertical supports;  $M_{sw}$  is the moment due to the self weight of the beam; and  $e$  is the eccentricity calculated by distance between plastic neutral axis of the composite beam and the pin of axial compressive load applicator.

Eccentricity  $e$  was determined by the following Equation (2).

$$e = \left( D_c + t_f + \frac{d_w}{2} \right) - y_c + \delta \tag{2}$$

where  $D_c$  is the slab thickness;  $t_f$  is the flange thickness;  $d_w$  is the height of the web;  $y_c$  is the depth of plastic neutral axis determined from the top of the slab; and  $\delta$  is the measured vertical deflection at the mid span.

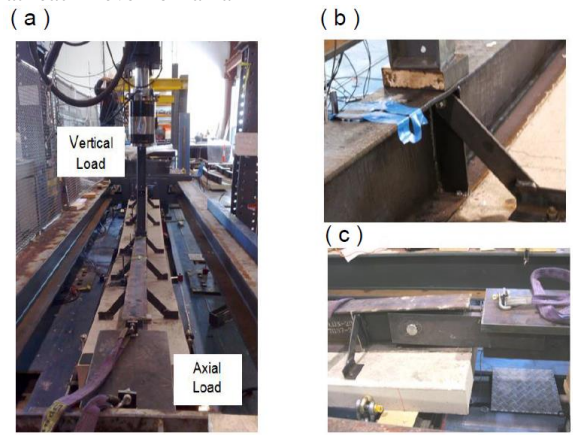


Figure 1 (a) Test set up for negative bending and axial compressive loads (b) Vertical load applicator (c) Axial Load applicator (Vasdravellis *et al.* 2012)

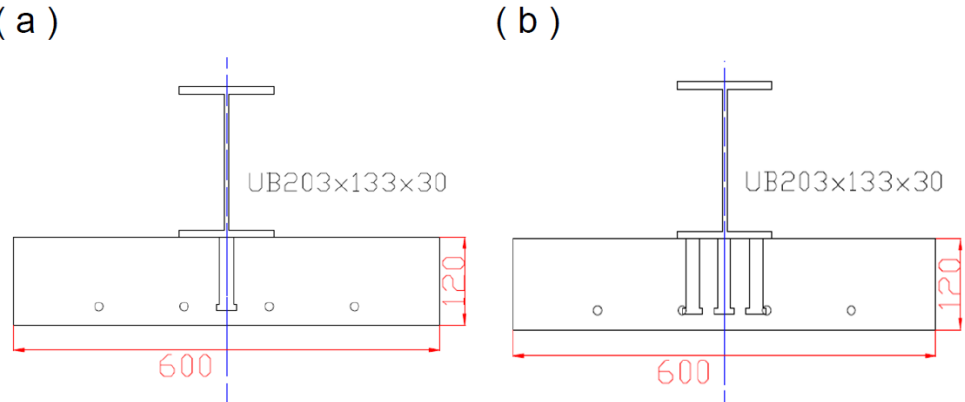


Figure 2 (a) Composite beam cross section in negative bending and compression (b) Composite beam cross section at both ends with three shear studs

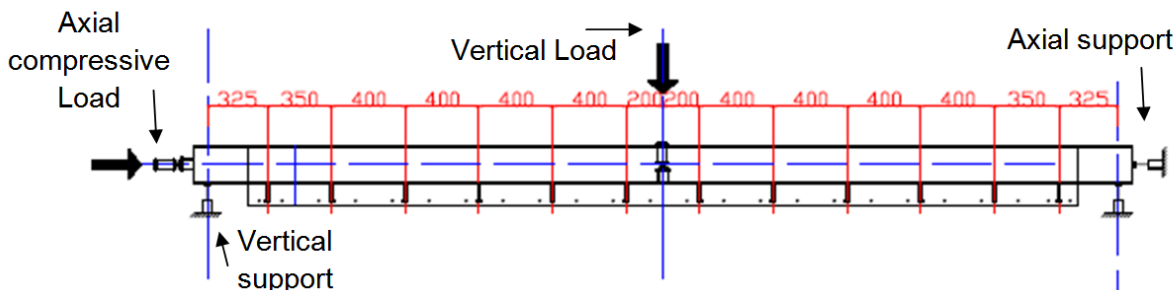


Figure 3 Details of test set-up of composite beam subjected to negative bending and axial compressive loads

Table 1 Experimental results of specimens CB1-CB6

Specimen	Ultimate moment (kNm)	Axial force (kN)	Failure mode
CB1	186	0	Ductile
CB2	140	256	Local buckling
CB3	166	718	Local buckling
CB4	132	1048	Local buckling
CB5	38	1801	Local buckling
CB6	11	2257	Local buckling

### 3.0 FINITE ELEMENT METHOD

#### 3.1 Concepts, element types, boundary conditions and interactions

The main concern was FEM modelling by using software Abaqus in order to obtain reliable results with non-linear effects of composite beam subjected to combined negative bending and axial compressive forces. Due to the complex contact interactions, binary axial loads and material non-linearity, the static implicit method was encountered convergence difficulties and thus, dynamic explicit method was used. It has been found that the dynamic explicit is more efficient in subjecting of convergence during large deformations, complicated contacts and material failures.

In order to obtain the accurate results with minimum computational time, half model was developed to each material component with considering its geometrical shapes. All components were assembled together in its symmetry on center line of the compressive axial loading direction similarly to experimental analysis. Developed typical finite element model, coordinate system used to load applications and selective meshes to each material components are indicated in Figure 4. While concrete slab was developed separately, the steel beam and shear studs were developed as one part with the consideration of its welding connection. The combinations of elements were chosen with considering computational cost and the accuracy of results. A three dimensional eight-node element with linear approximation of displacements, reduced integration with hourglass control, eight nodes and three translational degrees of freedom (C3D8R) was used to model concrete slab and solid shear stud material components by way of specific consideration in improving the convergence rate. With

considering high axial compressive load on steel beam, a three dimensional eight-node element with linear approximation of displacements, incompatible modes with hourglass control, eight nodes and three translational degrees of freedom (C3D8I) was applied to steel beam. A two-node linear three dimensional truss element with linear approximation of displacement, two nodes and three translational degrees of freedom (T3D2) was selected for wire mesh.

Quasi-static solution using Abaqus explicit dynamic solver was preferred due to the binary axial deformation and complicated contacts. Both vertical load and axial compressive load were applied by constant displacement method in each of particular time interval. Vertical load was concerned on center of steel beam same as experiment and axial compressive load was applied on the surface of steel beam. The uniform slow load application was needed owing to concrete material, which will fail in a sudden deflection. As a result, static results will be possible to evolve to dynamic results with the speed of the process and therefore, the analysis was ensured with different axial deformations in both directions to predict static results. In advance, smooth amplitude step was preferred to acquire more accuracy of results due to sudden impact load onto the deformed body even if constant velocity and to ensure gradual loading during ramping up and down from zero and to zero.

The FEM model was developed as much as possible to adopt all the exact behaviour of support conditions in experimental analysis. While axial load was applied on the surface of steel beam in FEM model, the nodes on the surface of another end of steel beam were resisted the displacement in the axial direction of steel beam. The roller supports were represented by resisting the displacement of nodes in the vertical direction at the developed model of steel beam with a clear span of 4950 mm same as the protection of vertical movement during experiments. The symmetry boundary condition was applied along the direction of composite beam by considering the implemented half model to facilitate a more economical solution. Boundary conditions are indicated in the Figure 5.

The contacts property in linking material components was decided according to the nature of the deformed body surfaces and actual characteristic activity of the contact nodes of deformed body in the experiment. Contact surfaces were selected according to the characteristics of surfaces that the master surface was selected as the surface of stiffer body and as the surface which contains coarser mesh. In defining contact property, surface-to-surface interaction property available in Abaqus was used by defining tangential behavior to consider friction & elastic slip and normal behavior to consider penetration and separation. Concrete slab and shear stud contact surfaces were selected to use surface-to-surface contact algorithm and the concrete slab was selected as master surface in the contact algorithm. Penalty friction formulation was

selected to its tangential behavior with the coefficient of 0.5 and the hard pressure over closure was selected to its normal behavior. In contact bodies of concrete slab and steel beam, the concrete slab, which is stiffer and contains coarse mesh, was selected as master surface by way of surface-to-surface contact algorithm with same tangential and normal behavior of slab and

stud contact surfaces. It was included with the separation behaviour for all material components in surface-to-surface contact algorithm as facilitated the real behaviour similarly experimental analysis. An embedded technique was used to define the bond of wire mesh and concrete slab.

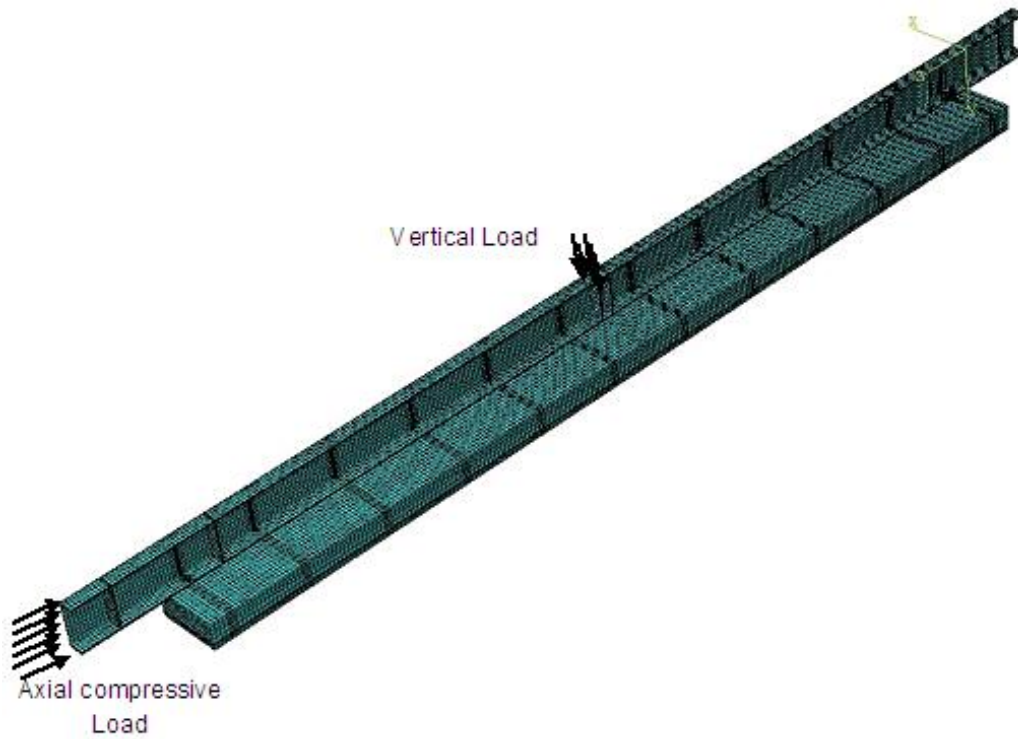


Figure 4 Finite Element meshes and load applications

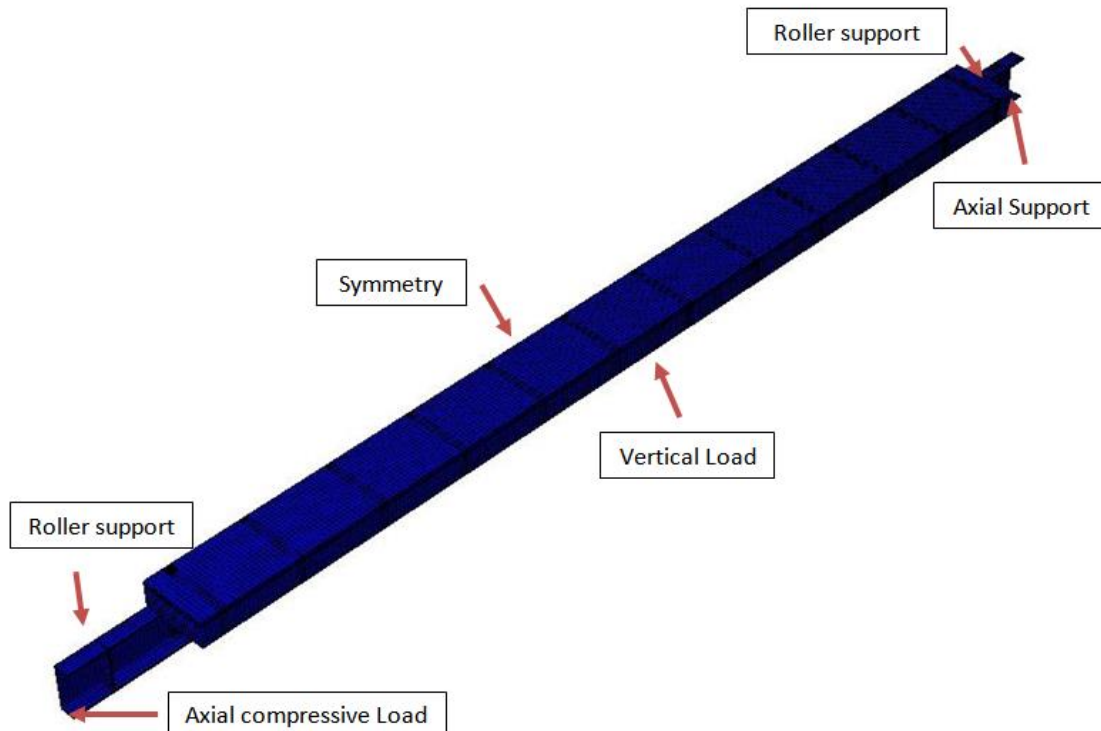


Figure 5 Finite Element model and coordinate system used for the boundary conditions

In addition, the difference between support reaction forces and applied forces was compared to ensure the accuracy of results. The quasi-static analysis was made with Abaqus explicit dynamic solver by preserving the energy balances that the kinetic energy of deformed model was maintained with a small fraction of its internal energy countered lesser than 5% during full time of simulations.

### 3.2 Material models

Concrete damaged plasticity model is available in Abaqus for concrete material model, which simulates crushing under compression and cracking under tension with tension stiffening and shear capacity of cracked concrete. The degradation mechanisms of the hardening variables are characterized in controlling the evolution of failure both under crushing and under tension with evaluation of yield surface hardening

variables proposed by Lubliner *et al.* [18]. The strength hypothesis and parameters of concrete were recommended by Kmiecik and Kaminski [19], which are 36 of dilatation angle, 0.1 of eccentricity, 1.16 of ratio of biaxial and uniaxial state strength, 0.6667 of ratio of distance between the hydrostatic axis and deviatoric cross section and zero of viscosity. While using the same parameters for biaxial material property of concrete, the compressive and tensile behavior were developed and applied with using the ultimate state values of experiment proposed by Desay & Krishnan [20] and Eurocode formula, respectively. Material tests were performed by Vasdravellis *et al.* [12-13] in the same day of experiment for each composite beam and the ultimate limit stress-strain values were provided. The developed stress-strain values of concrete in compression and tension for FEM are illustrated in Figure 6(a) and Figure 6(b), respectively.

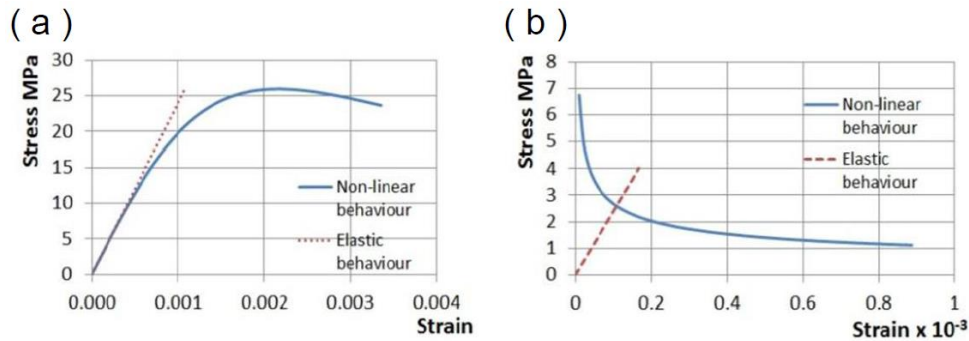


Figure 6 (a) Concrete material in compression (b) Concrete material in tension

Elastic state of concrete was determined by Eurocode formula mentioned as Equation (3) with 0.2 of Posion’s ratio. Where  $E_{cm}$  is longitudinal modulus of elasticity and  $f_{cm}$  is compressive strength. First 40% of ultimate stress value was taken as elastic state and plastic state was developed by Equation (4) of Desay & Krishnan [20] in compressive behaviour of concrete as shown in Figure 6(a). Where  $E_c$  is longitudinal modulus of elasticity,  $\sigma_c$  is compressive stress,  $\dot{\epsilon}_c$  is strain and  $\dot{\epsilon}_{c1}$  is strain at peak point. Abaqus manual further suggests that the plastic strain will be taken as inelastic strain due to the absence of compression damage variables and thus, compression damage was avoided in the input data. While using elastic behavior with Equation (5), the exponential function is a most convenient function for appropriate results after cracking in fracture energy concept and it was used by Equation (6). The developed stress-strain responses of concrete in tensile state are shown in Figure 6(b). Where  $E_c$  is longitudinal modulus of elasticity,  $\sigma_t$  is tensile stress,  $\dot{\epsilon}_{cr}$  is strain at concrete crushing and  $\dot{\epsilon}_t$  is tensile strain. Tension damage parameters in the cracking behaviour of concrete were developed with strain responses by Equation (7).

Structural steel beam characteristics were considered in the behavior of von Mises yield criterion with isotropic hardening rule (bilinear-hardening material) in order to prefer for large strain analysis proposed by Gattesco (1999) [22] as indicated in Figure 7. An approach was followed by three states of stress-strain behaviour which of elastic state, perfectly plastic state and nonlinear state with hardening variables. The relationship of stress-strain in elastic state of curve was represented from the origin with positive stress-strain values and slope of curve was taken as elastic modulus of the steel beam material by means of Equations (8).

$$E_{cm} = 22(0.1f_{cm})^{0.3} \tag{3}$$

$$\sigma_c = \frac{E_c \dot{\epsilon}_c}{1 + \left[\frac{\dot{\epsilon}_c}{\dot{\epsilon}_{c1}}\right]^2} \tag{4}$$

$$\sigma_t = E_c \dot{\epsilon}_t \text{ if } \dot{\epsilon}_t \leq \dot{\epsilon}_{cr} \tag{5}$$

$$\sigma_t = f_{cm} \left[\frac{\dot{\epsilon}_{cr}}{\dot{\epsilon}_t}\right]^{0.4} \text{ if } \dot{\epsilon}_t > \dot{\epsilon}_{cr} \tag{6}$$

$$\tilde{\epsilon}_t^{pl} = \tilde{\epsilon}_t^{ck} - \frac{d_t}{(1-d_t)} \frac{\sigma_t}{E_0} \tag{7}$$

where  $E_s$  is Elastic modulus of steel and  $\sigma_s$  and  $\dot{\epsilon}_s$  are stress and strain variables, respectively. According to Gattesco (1999) [22], it was started then linearly and perfectly plastic from specified yield stress to the position stated as beginning of strain hardening with Equation (9). where  $f_{sy}$  is yield stress of steel beam. The curve was continued with Equation (10) until its ultimate stress-strain value, which depended on steel ductility. where  $\sigma_y$ ,  $\dot{\epsilon}_s$ ,  $f_{sy}$  and  $f_{su}$  are variable stress, variable strain, yield and ultimate stress, respectively and  $\dot{\epsilon}_{sh}$  is strain at the beginning of hardening stage of steel beam. Value of  $k$  was defined with the Equation (11) and the value of  $k_s$  was given as 0.028 in Gattesco, 1999 [22].

$$\sigma_c = E_s \dot{\epsilon}_s \tag{8}$$

$$\sigma_y = f_{sy} + (f_{su} - f_{sy}) \left[1 - e^{-\left[\frac{(\dot{\epsilon}_{sh} - \dot{\epsilon}_s)}{k}\right]}\right] \tag{9}$$

$$k = k_x \frac{(\dot{\epsilon}_{sh} - \dot{\epsilon}_{su})}{(\dot{\epsilon}_{sh} - 0.16)} \tag{10}$$

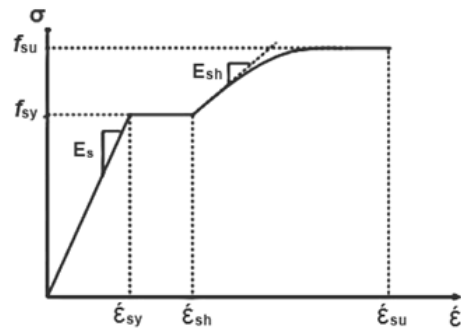


Figure 7 Stress strain curve of steel beam

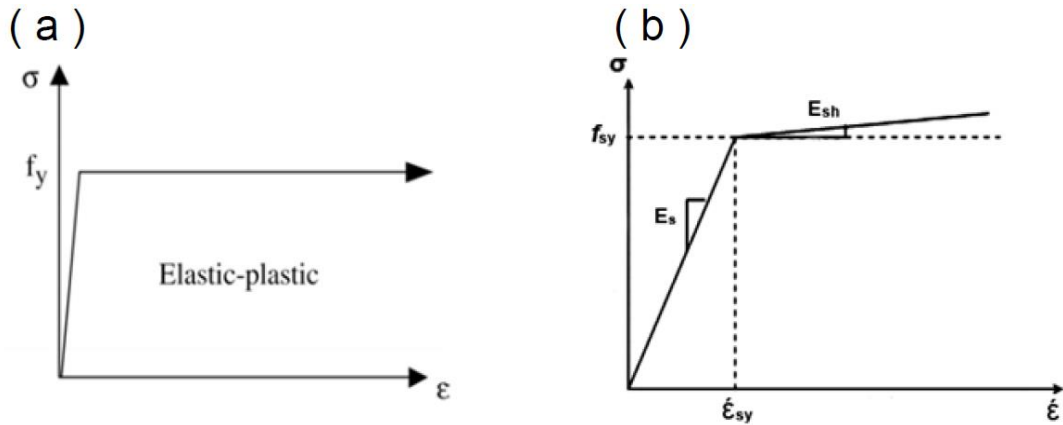


Figure 8 (a). Simplified stress strain curve for shear studs, (b). Stress strain curve for reinforcing bars

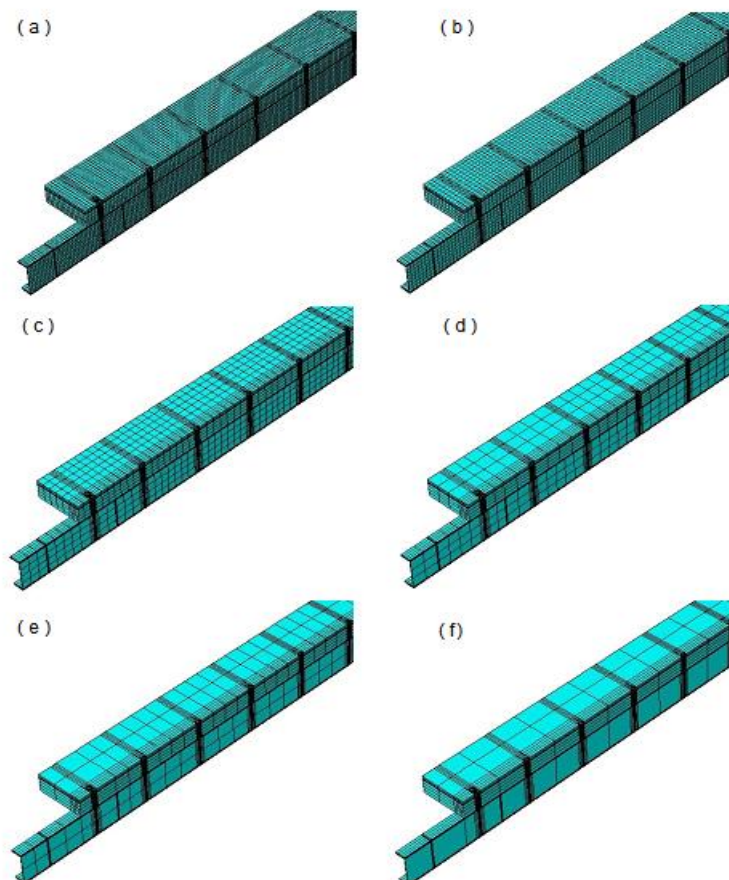


Figure 9 Mesh Configuration for concrete slab and steel beam (a) Mesh A (18×18, 18×18) (b) Mesh B (24×24, 24×24) (c) Mesh C (50×50, 50×50) (d) Mesh D (75×75, 75×75) (e) Mesh E (100×100, 100×100) (f) Mesh F (150×150, 150×150), Sizes denotes to concrete slab and steel beam respectively

Simplified stress and strain characteristics were used for shear stud as shown in Figure 8(a). The behaviour was at initial with elastic modulus until its ultimate yield stress of shear studs and afterward it was defined with tangent modulus by value of zero. Material stress-strain characteristics of reinforcing bars were followed with bilinear stress-strain curve as shown in Figure 8(b). The behaviour was as elastic at the beginning stage and afterward, it was considered as yielding with strain hardening characteristics by means of piecewise linear laws. The constitutive law was used to be satisfactorily accurate the plastic flow and isotropic hardening with considering by means of Mises plasticity.

### 3.3 Mesh size sensitivity discretizations

Mesh configurations were considered to each material component as coarse, medium and fine meshes. In this case of study, it was observed that mesh discretizations are a sensitivity issue due to biaxial deformation with non-linear simulations. Biaxial large deformation creates the mesh distortion and it needs to be regulated by minimizing and controlling the distortion of elements for accurate results. Meantime, concrete is a brittle material and it will behave enormously in a small deformation. Moreover, axial compression creates excess slip between concrete slab and steel beam components. Thus, these issues have been deeply taken to consider with mesh discretizations by way of comparing load-deflection responses and material failure similarity between experimental and FEM model results.

In terms of studies about mesh discretizations in the behaviours of local and global responses and in the effects of stretching and distortion of elements due to explicit solver, six mesh configurations were selected to concrete slab and steel beam and the studies were made about its margins of errors in the load-deflection responses. The components are scaled in mm for mesh creations and those are (18×18, 18×18), (24×24, 24×24), (50×50, 50×50), (75×75, 75×75), (100×100, 100×100) and (150×150, 150×150), which of mentioned concrete slab and steel beam, respectively and named as Mesh A to Mesh F. Figure 9 (a) to Figure 9 (f) are shown the Mesh A to Mesh F. Finally, the meshes were fixed to each component with considering reasonable time increments and with identical results of FEM. Large shear forces are necessary to be transmitted from steel beam to concrete slab in shear studs particularly a small mechanical device and as a result, high concentrated forces will be formed to the meshes of shear studs. Combined axial compressive loads and vertical loads also will create excess deformation on the stud elements. Even though, adequate results were possible with various meshes to shear studs, the fine mesh was selected with the consideration of all aspects. The shear stud mesh is shown in Figure 10.

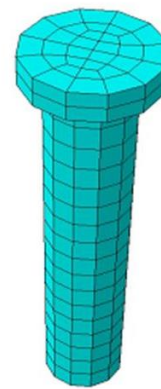


Figure 10 Mesh Configuration for Shear stud (5×5)

## 4.0 RESULTS AND DISCUSSION

The composite beam studied above has been provided experimental data by Vasdravellis *et al.* [12-13]. The FEM model was developed to predict the ultimate limit state in the hogging region of steel-concrete composite beam subjected to compressive forces on steel section. The numerical simulation was carried out in this study by considering contact algorithms and all fracture aspects in material components to achieve real behaviours with comparison to experimental features. Due to the complex contact behaviours and combined forces in multi directions, explicit solver was used to calibrate against the corresponding experimental data. Initially, monotonic vertical and axial load were applied to composite beam and the results were compared with experimental results. The optimum speed determined as 0.5 and 0.12 mm/s of vertical and axial loadings, respectively, was taken with comparing distortion in elements, load-deflection responses and material fracture behaviours. Various speeds within the limitation of optimum speed were then applied in both direction and necessary combination of load was predicted with proper limiting moment and axial compressive load values. Further, the results were checked for static results with various parameters known as speed and energy stabilities. Meantime, the convergence study was included due to sensitivity of meshes and adequate results were predicted with considering margins of errors in every simulation.

In convergence studies, vertical load-deflection response and axial load-deflection response were plotted with different sizes of mesh A to F as shown in Figure 11 (a) and 11 (b), respectively. While appropriate concurrences were observed in mesh A to E in axial load-deflection response curve, mesh A and B only were tallied with appropriate concurrences in vertical load-deflection response curve. Similarly, appropriate concurrences were observed in mesh A and B at moment-axial load response curve and moment-vertical load response curve as shown in Figure 11(c) and Figure 11(d), respectively. Even though, mesh A and B were in very close agreement to each other, more fine mesh A was selected to investigate further studies due to consider its clear yielding progression of the steel beam.

Quasi static solution is essential in explicit solver with energy stabilities. Quasi static solution limits the kinetic energy of the system to a small value throughout the analysis. Because of materials failures, sudden drops of the load carrying capacity increase kinetic energy of the system enormously. The perfect slow displacements in each direction of loads were found after checking with many trials and those were applied to the FEM

models. There is possible to sudden raise in the kinetic energy at the initial point. As a result, smooth amplitude function was used to control the kinetic energy throughout the analysis. Figures 12 (a) and (b) are indicated on the subject of the controlled kinetic energy with internal energy. It is clearly visible from Figure 12 (a) that the kinetic energy was very low

and almost negligible throughout the analysis comparing with internal energy. Meantime, the Figure 12(b) states that the kinetic energy was controlled at the initial point within 4.1% of internal energy by speed control with smooth amplitude function.

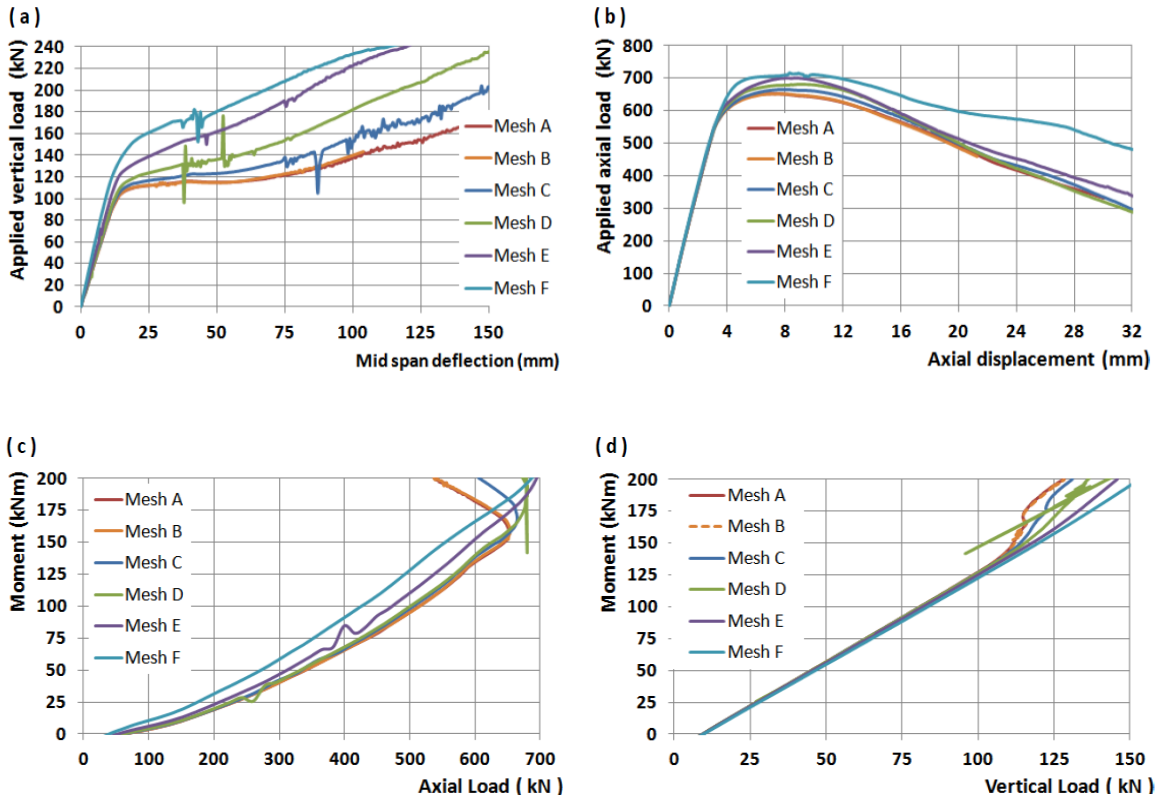


Figure 11 Results of mesh sensitivity study of composite beam subjected to combine load(a) Response of applied vertical load and mid-span deflection (b) Response of applied axial load and axial displacement (c) Response of moment and axial load (d) Response of moment and vertical load

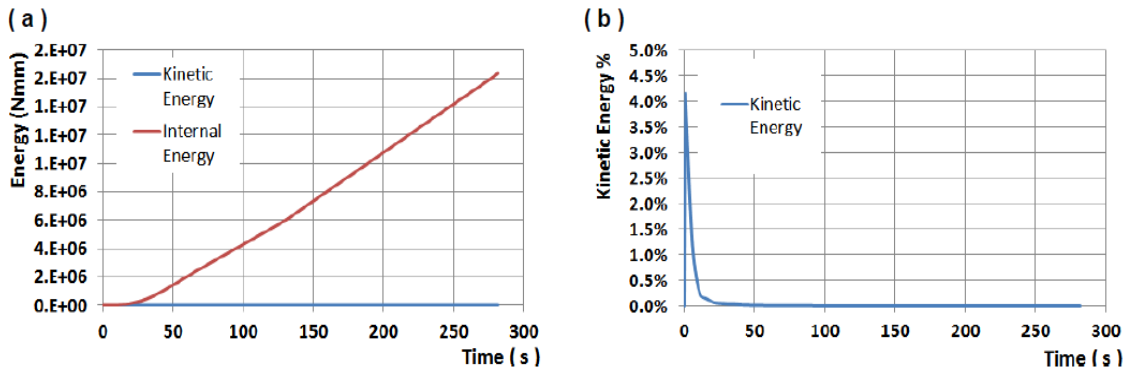


Figure 12 Structure control system (a) Comparison of internal and kinetic energy (b) Kinetic energy throughout the analysis

Improper fluctuation in load-deflection responses was possible due to biaxial loads in this case. Therefore, displacement control was only easily persuaded. Numbers of simulations were made with various speeds and within the limitation of deformation speeds, which were already derived. Perfect augmentations in load and deformation of both axes were only taken for further studies. The found rate of vertical and axial loadings in this case is shown in Figure 13 (a) and axial deformation rate is shown in Figure 13 (b). Figure 13 (a) shows that both axial and vertical directions were positively

deformed in their respective directions and meanwhile, Figure 13 (b) shows that axial deformed speed was within the limitation, which was already derived. The total forces applied in each direction of specimen were calculated by summing up the reaction forces of nodes in both directions. Moreover, applied load and support reaction forces were compared for the verification of static state analysis. The comparison of vertical applied load-support reaction forces and axial applied load-support reaction forces are exposed in Figure 14 (a) and Figure 14 (b), respectively.

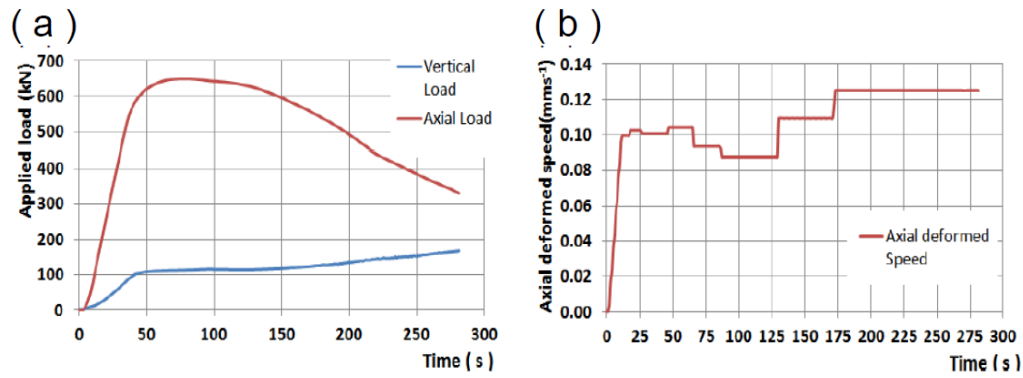


Figure 13 Structure control system (a) Rate of applied vertical and axial load (b) Axial deformation rate

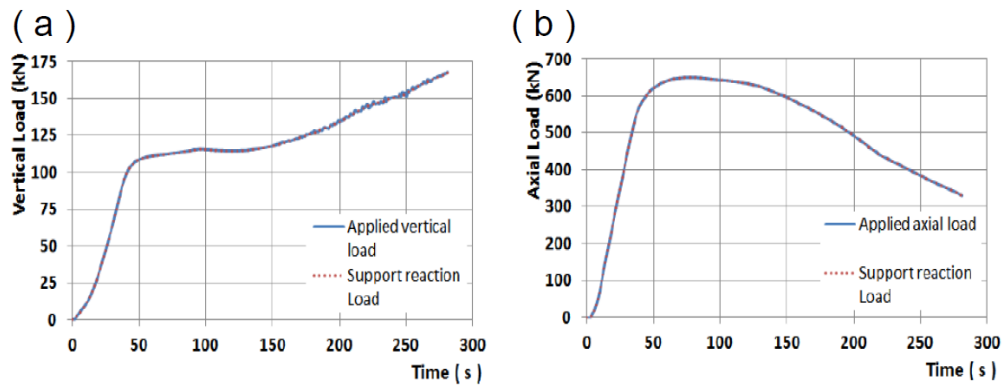


Figure 14 Structure control system (a) Comparison of applied and support reaction forces in vertical direction (b) Comparison of applied and support reaction forces in axial direction

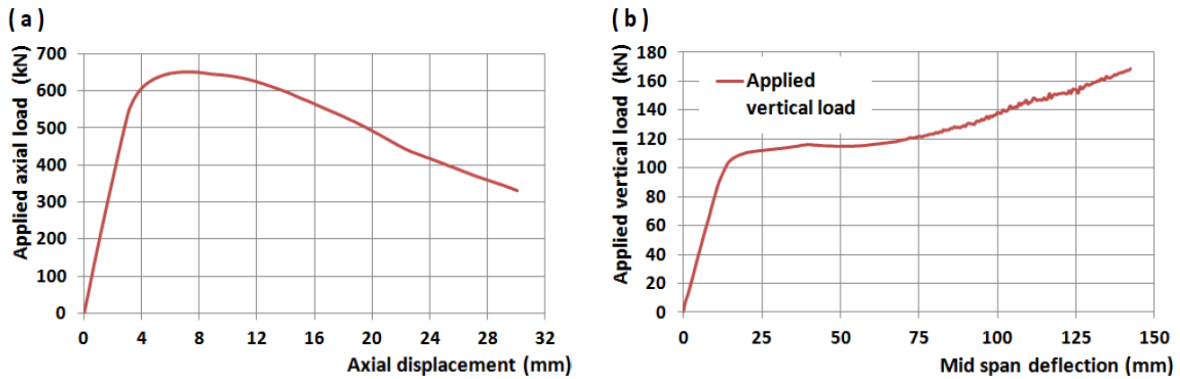


Figure 15 (a) Applied axial load-axial displacement responses (b) Applied vertical load-Mid span deflection responses

The applied axial load-axial displacement and applied vertical load-mid span deflection curve are shown in Figure 15 (a) and Figure 15 (b), respectively. The ultimate axial load capacity of the specimen was in a very small axial displacement and thus, it was very small displacement rate applied in axial direction with smooth amplitude function. When the axial compressive load was 651.54 kN, the specimen was reached its failure state by high yielding of web in steel beam before other material components reached its ultimate stress values. It was confirmed by stress contours in shear studs area and its surrounding areas of concrete that there was no yielding or crushing, respectively. There was no reinforcement fracture in that area until the axial compressive load reached its limit state value. The shear connection was capable after the specific ultimate limit state behaviour reached, which were determined

by axial load with bending moment and thus, the vertical load was still increased.

The ultimate moment was determined with the Equation (1) and Equation (2). The stage of FEM analysis where maximum ultimate limit axial load reached was stated as ultimate limit state of composite beam when the composite beam subjected to combined negative bending and axial load. The vertical load and mid-span deflection at the time level of increment where the axial load was reached its maximum, were taken for the determination of moment. The moment-time curve, moment-vertical load curve and moment-axial load curve are shown in Figure 16 (a), 16 (b) and 16 (c), respectively. The comparison of ultimate limit values between FEM model and experiment provides respective results and those were plotted in Figure 16 (d). It can be observed that the axial load and moment values at ultimate limit state was reasonably well with the experimental

limit state values. The experimental axial load and moment at ultimate limit state were 718kN and 166kNm, respectively, and the values predicted by FEM model were 651.54kN and 158kNm, respectively. The difference between the limit state values of experiment and FEM model was within 10 %. The axial load and moment at ultimate limit state obtained from FEM model by means of experimental values were 91 % and 95 %, respectively, with corresponding coefficient of variation of 0.09 and 0.05, respectively.

Correspondingly, the failure behaviour in each material component was analysed with every level of time increment of FEM model. The concrete slab response in tensile behaviour criteria until the composite beam reached its ultimate limit state with observed cracks in the stress contours at two locations of concrete slab and those are provided in Figure 17 (a) to (e). Due to the concrete damaged plasticity model, which was used with crushing and cracking variables in this FEM model, it was facilitated to study the fractured criteria in concrete. The initial failure in concrete was observed in FEM model when the combination of axial load is 575 kN and the moment is 123 kNm. The orange and red colours in the stress contours denote

the cracking regions and green colour denotes the unyielding regions. These cracks were flexural cracks and crack zone was increased rapidly. The Figure 17(c) to (e) demonstrate in order to explain the crack initiation and propagation in those regions at every level of combination of axial load and moment, which are (650 kN, 154 kNm), (651 kN, 158 kNm) and (641 kN, M=168 kNm), respectively.

It was important to study the behaviour of composite beam with failure prediction due to applied load on steel section and therefore, the elastic-plastic model was used to structural steel beam in the behavior of Von Mises yield criterion with isotropic hardening rule. Von Mises stress contour of yielding criteria of steel beam are shown in Figure 18 and Figure 19, respectively. The initial yielding in web of steel beam of FEM model was at the combination of 575 kN of axial load and 75 kNm of moment as shown in Figure 18. The stresses in web were gradually increased and continuously, the FEM results were predicted the extensive yielding in the web of steel beam at the axial load and moment combination of 651.54 kN and 158 kNm, respectively. The Figure 19 (b) shows the extensive yielding of web of steel beam.

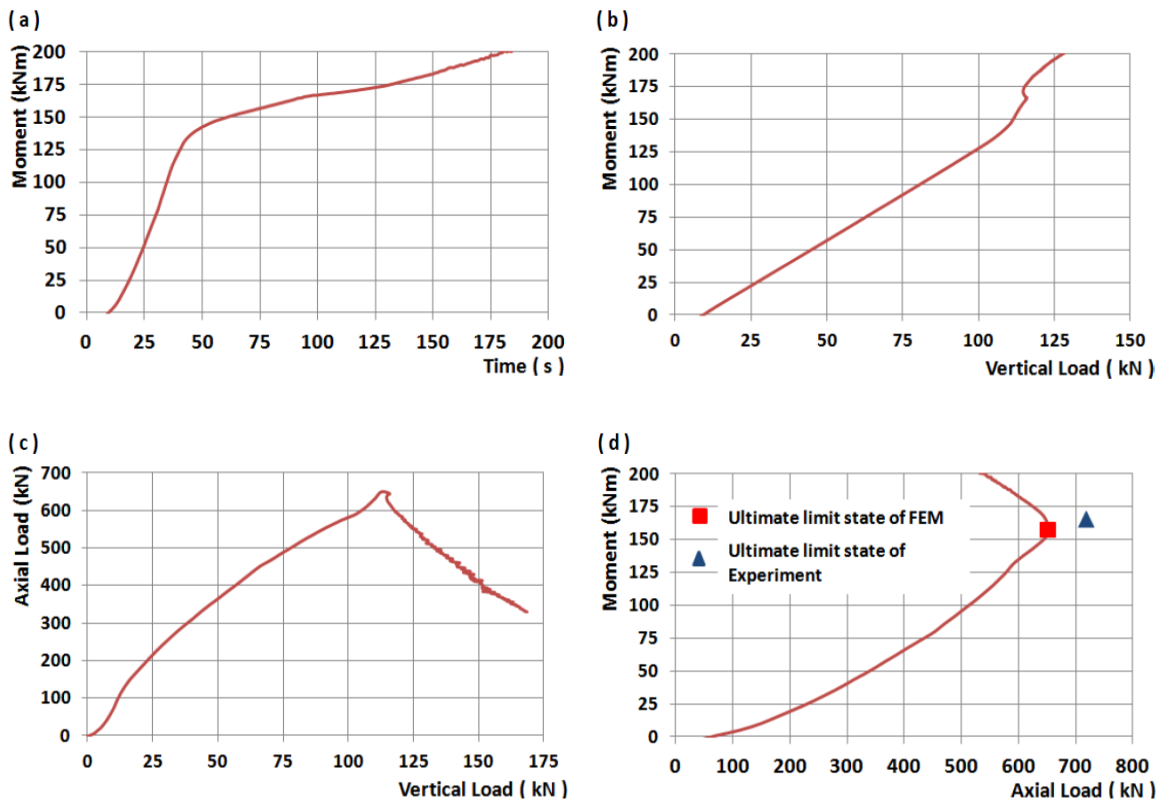
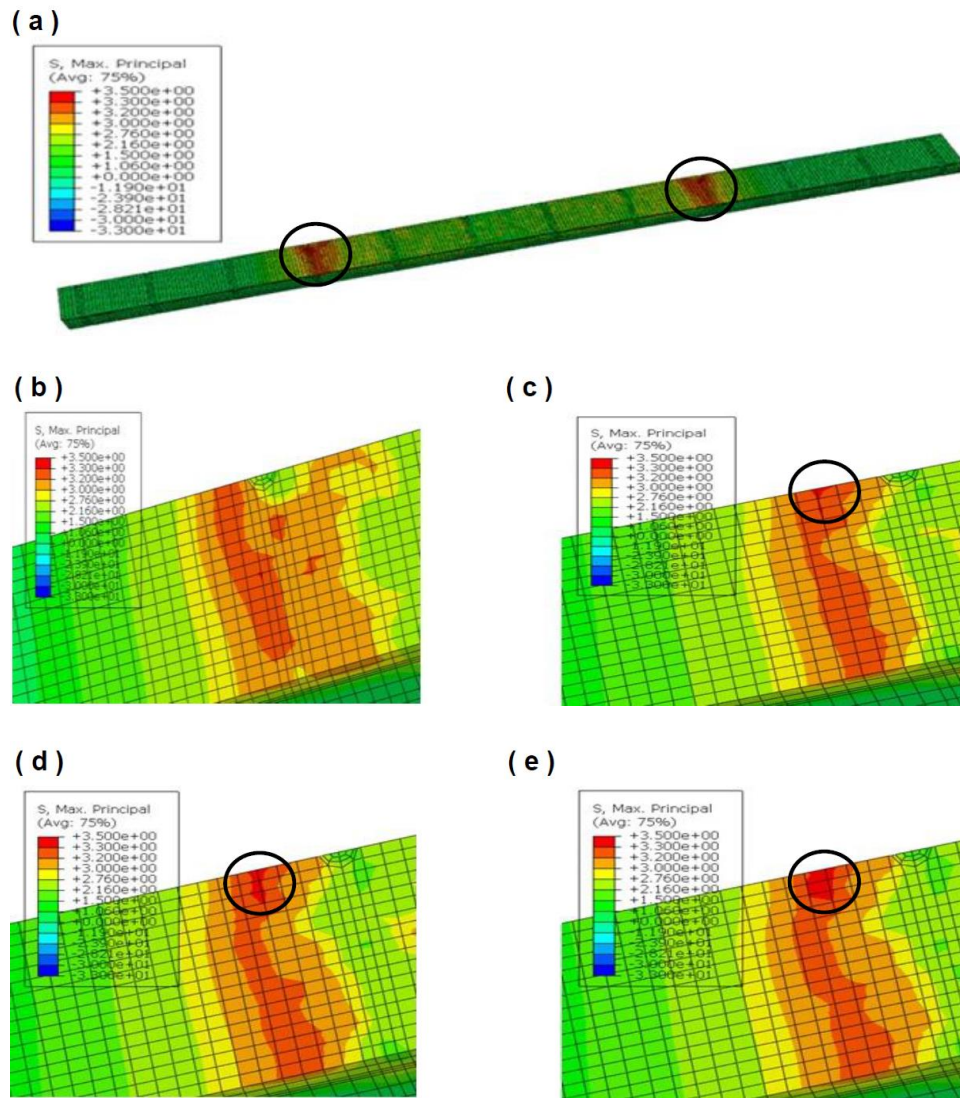
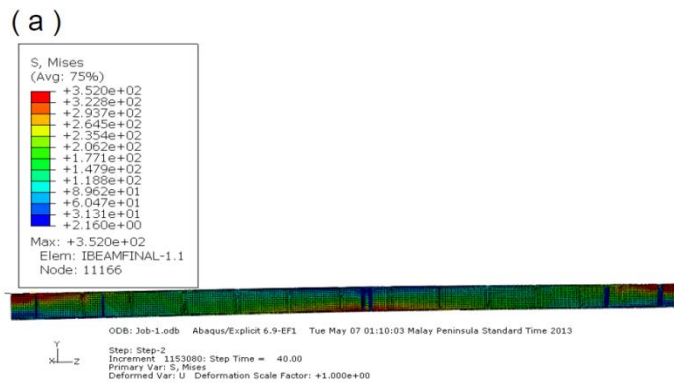
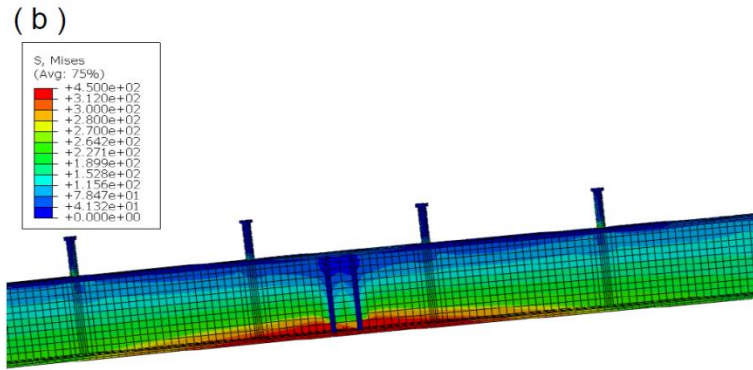


Figure 16 Ultimate state (a) Moment-time response (b) Moment-vertical load response (c) Moment-axial load response(d) Comparison of FEM and experiment at ultimate state



**Figure 17** Concrete cracking behaviour (a) Yielding region (b) Max Principle contour at AL= 575 kN, M=123kNm (c) Max Principle contour at AL=650 kN, M=154kNm (d) Max Principle contour at AL=651 kN, M=158 kNm (e) Max Principle contour at AL=641 kN, M=168 kNm, AL denotes axial load and M denotes moment, AL denotes axial load and M denotes moment





**Figure 18** Steel beam yielding progression in earlier state at 575 kN of axial load and 75kNm of moment (a) Steel beam yielding area (b) Steel web yielding

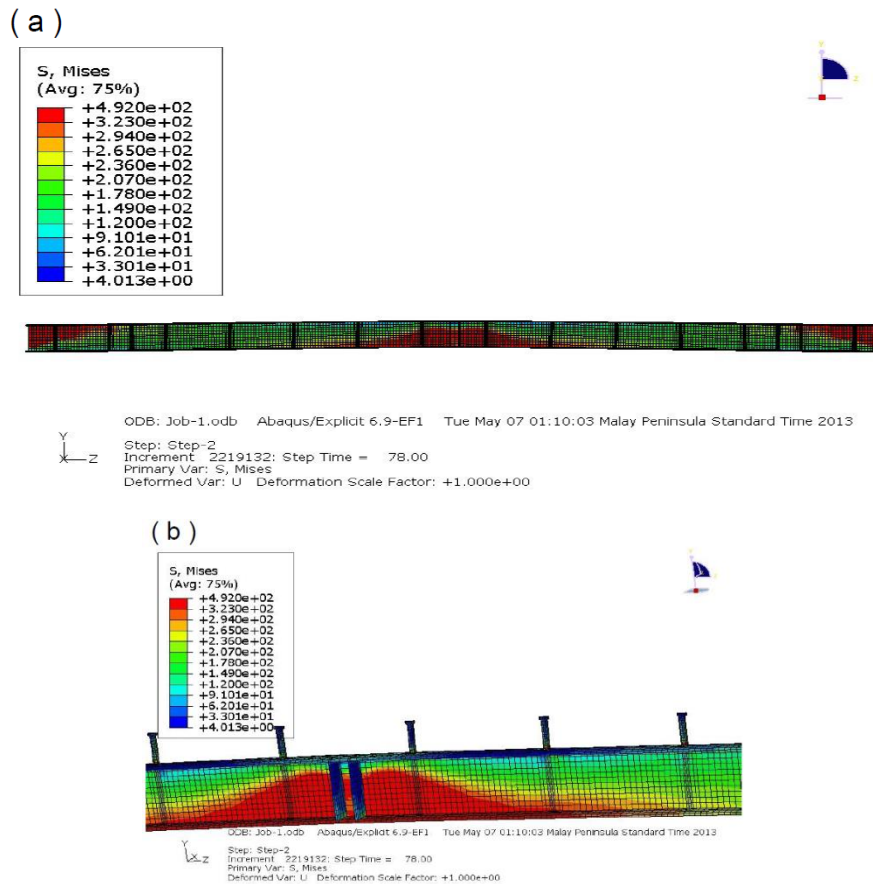


**Figure 19** Steel beam yielding progression in failure state at the values 651.54 kN of axial load and 158kNm of moment (a) Steel beam yielding area (b) Steel web extensive yielding

**5.0 CONCLUSION**

This paper has studied thoroughly the finite element method (FEM) analysis of steel-concrete composite beam subjected to combined negative bending and axial compressive load with considering real contact behaviours and material nonlinearities. Available experimental data were used to verify the reliability of FEM model. The following conclusions are obtained from FEM analysis in implementation of FEM model of composite beam due to combined loadings.

1. The model has been tested with low-velocity impacts in combined loads which compared very well with numerical

results using ABAQUS explicit solver. It was found that the optimum speeds, which are 0.50 and 0.12 mm/s of vertical and axial compressive loadings, respectively, give better results by means of computing in distortion of elements, load-deflection responses and materials fracture behaviours.

2. Mesh size sensitivity discretizations create the strain values enormously in the ABAQUS explicit solver. The proper discretizations meshes are necessary to find for all geometry in the prediction with better distortion control.
3. The failure mode of composite beam subjected to combined negative bending and axial compressive loads

was due to excess yielding and buckling of web of steel beam. It was found that the yielding of steel beam by the direct influence of axial compressive load decreases the stiffness of section and it leads to failure. The high stresses occur at web of steel beam and some regions of concrete in whole material components. Meanwhile, the different levels of axial compressive load give different ultimate state values and different failure modes.

4. The peak at the time increment levels of FEM has been predicted by axial compressive load-displacement curve with the failure mode observed as buckling of web and it was determined as the limit state of composite beam. The combination of axial compressive load and ultimate limit bending moment is presented as 651.54 kN and 158 kNm, respectively in FEM analysis and those are with corresponding coefficient of variation of 0.09 and 0.05, respectively in the comparison of experimental values. By these relevant results, it could be concluded that these modelling techniques of composite beam can be used for different level of axial compressive load and moment combinations in practice.
5. This FEM is suggested for further applications in practice in the conception of postponing the failure states of composite beam by locally strengthening with stiffness due to influence of axial compressive loads for more various general cases.

Further, these FEM techniques can be used to predict the limit state behaviours of large models with the influences of material uncertainties and large cost involved models of experimental programs with biaxial constraints.

### Acknowledgement

The authors wish to thank University Kebangsaan Malaysia (UKM-GGPM- NBT-029-2011 and UKM-GUP-2011-067) for their financial assistance of this research.

### References

- [1] Nie, J., Luo, L., Hu, S. 2000. Experimental Study On Composite Steel-Concrete Beams Under Combined Bending and Torsion. *Composite and Hybrid Structures*. 2: 631–8.
- [2] Tan, E. L., Uy, B. 2009. Experimental Study on Straight Composite Beams Subjected to Combined Flexure and Torsion. *J Constr Steel Res*. 65: 784–793.
- [3] Tan, E. L., Uy, B. 2009. Experimental Study on Curved Composite Beams Subjected to Combined Flexure And Torsion. *J Constr Steel Res*. 65: 1855–1863.
- [4] Mirza, O., Uy, B. 2010. Effects of the Combination of Axial and Shear Loading on the Headed Stud Steel Anchors. *Engineering Structures*. 32: 93–105.
- [5] Elghazouli, A. Y., Treadway, J. 2008. Inelastic Behaviour of Composite Members Under Combined Bending and Axial Loading. *J Constr Steel Res*. 64: 1008–1019.
- [6] Loh, H. Y., Uy, B., Bradford, M. A. 2004. The Effects of Partial Shear Connection in the Hogging Moment Regions of Composite Beams; Part 11- Experimental study. *J Constr Steel Res*. 60: 897–919.
- [7] Loh, H. Y., Uy, B., Bradford, M. A. 2004. The Effects of Partial Shear Connection in the Hogging Moment Regions of Composite Beams; Part 1- Analytical study. *J Constr Steel Res*. 60: 921–962.
- [8] Vasdravellis, G., Uy, B., Tan, E. L., Kirkland, B. 2012. The Effects of Axial Tension on the Hogging Moment Regions of Composite Beams. *J Constr Steel Res*. 68: 20–33.
- [9] Vasdravellis, G., Uy, B., Tan, E. L., Kirkland, B. 2012. The Effects of Axial Tension on the Sagging-Moment Regions of Composite Beams. *J Constr Steel Res*. 72: 240–253.
- [10] Basker, K., Shanmugam, N. E. 2003. Steel Concrete Composite Plate Girders Subject to Combined Shear and Bending. *J Constr Steel Res*. 59: 531–557.
- [11] BS EN 1994-1-1, Euro Code 4; 2004. Design of Composite Steel and Concrete Structure; Part 1.1; General Rules and Rules for Buildings. London (UK); British Standards Institution.
- [12] Vasdravellis, G., Uy, B., Tan, E. L., Kirkland, B. 2012. Behavior and Design of Composite Beams Subjected to Negative Bending and Compression. *J Constr Steel Res*. 79: 34–47.
- [13] Vasdravellis, G., Uy, B., Tan, E. L., Kirkland, B. 2012. Behaviour and Design of Composite Beams Subjected to Negative Bending. Proc. of the 10th Intl. Conf. on Advances in Steel Concrete Composite and Hybrid Structures. 427–434.
- [14] Tan, E. L., Uy, B. 2011. Nonlinear Analysis of Composite Beams Subjected to Combined Flexure and Torsion. *J Constr Steel Res*. 67: 790–799.
- [15] Tahmasebinia, F., Ranzi, G., Zona, A. 2013. Probabilistic three-dimensional Finite Element Study on Composite Beam with Steel Trapezoidal Decking. *J Constr Steel Res*. 80: 394–411.
- [16] Qureshi, J., Lam, D., Ye, J. 2011. Effects of Shear Connectors Spacing and Layout on the Shear Connector Capacity in Composite Beam. *J Constr Steel Res*. 67: 706–719.
- [17] Thevendran, V., Chen, S., Shanmugam, N. E., Liew, J. Y. R. 1999. Nonlinear Analysis of Steel Concrete Composite Beams Curved in Plan. *Journal of Finite Elements in Analysis and Design*. 32: 125–139.
- [18] Lubliner, J., Olive, J., Oller, S., Onate, E. 1989. A Plastic-damage Model for Concrete. *International Journal of Solids and Structures*. 25: 299–329.
- [19] Kmiecik, P., Kaminski, M. 2011. Proceedings of Conference on Modelling of Reinforced Concrete Structures and Composite Structures with Concrete Strength Degradation Taken Into Consideration in Archives of Civil and Mechanical Engineering VI, Wroclaw, Poland. 623–636.
- [20] Desayi, P., Krishnan, S. 1964. Equation for the Stress-Strain Curve of Concrete. *ACIJ Proceed*. 61(22): 345–350.
- [21] Gattesco, N. 1999. Analytical Modelling of Nonlinear Behavior of Composite Beams with Deformable Connection. *J Constr Steel Res*. 52: 195–218.
- [22] ABAQUS user's manual, version 6.11, Dassault Systèmes, Simulia Corp., Providence, RI, USA.